Catalysis Science & Technology

PAPER

View Article Online
View Journal | View Issue

Cite this: *Catal. Sci. Technol.*, 2018, 8, 6143

Effect of acidity and ruthenium species on catalytic performance of ruthenium catalysts for acetylene hydrochlorination†

Xiaolong Wang, Guojun Lan, Huazhang Liu, Yihan Zhu and Ying Li *

Received 13th August 2018,
Accepted 22nd October 2018

DOI: 10.1039/c8cy01677a

rsc.li/catalysis

Carbon-supported ruthenium catalysts are promising mercury-free catalysts for acetylene hydrochlorination, due to their high activity and relatively low price. However, ruthenium catalysts often suffer from serious deactivation. Herein, a stable $RuCl_3$-A/AC catalyst was prepared by applying a simple ammonia treatment during the impregnation process. The fresh and used ruthenium catalysts were comprehensively characterized using N_2 sorption, NH_3-temperature-programmed desorption (NH_3-TPD), H_2 temperature-programmed reduction (H_2-TPR), thermogravimetric analysis (TGA), and X-ray photoelectron spectroscopy (XPS). The results show that the $RuCl_3$ species is identified as the active species, and the surface acidity of the $RuCl_3$/AC catalyst is generated mainly from supported $RuCl_3$ species, which can easily cause coke deposition. The enhancement of the stability of the $RuCl_3$-A/AC catalyst is attributed to the formation of RuO_x species and the decrease of the surface acidity.

1 Introduction

Vinyl chloride monomer (VCM) is a major chemical intermediate in the manufacture of polyvinyl chloride (PVC), which is the third most important polymer in use today.[1] At present, VCM is generally synthesized *via* hydrochlorination of acetylene in regions of the world where coal is abundant, especially in China. However, production of VCM in acetylene hydrochlorination units consumes about 1400 tons of mercury, which causes serious environmental problems. With the implementation of mercury restrictions, the substitution of mercury is one of the key challenges for vinyl chloride production *via* acetylene hydrochlorination.[2] Therefore, mercury-free catalysts for acetylene hydrochlorination have been extensively researched.[3,4] Hutchings' group reported a relationship between the catalytic performance and the standard electrode potential of a cationic catalyst, and predicted that a gold catalyst would be a good candidate for acetylene hydrochlorination.[5,6] Since then, Au catalysts have been intensively studied.[7–9] Although Johnson Matthey technology has achieved the successful commercialization of gold catalysts with low loading in 2016,[6] gold has not been widely applied in chloride alkali plants due to its high cost. Therefore, Ru-based catalysts, which are much less expensive and possess high activity, are considered to be another promising candidate for acetylene hydrochlorination.[10] However, the general activity of Ru-based catalysts is relatively lower than that of Au-based catalysts. Therefore, many efforts have been dedicated to enhancing their catalytic activity, such as adding another metal or ionic liquids,[11–17] using heteroatom-doped carbon supports,[18–23] and using other Ru salts rather than $RuCl_3$.[24–26] RuO_2, $RuCl_3$ and Ru/RuO_y species have been suggested to be the active species in ruthenium catalysts, as reported by Li.[27] Zhang *et al.* prepared a series of ruthenium–cobalt catalysts, and found that the Co cobalt additive can greatly influence the amount of ruthenium species, which results in good catalytic activity.[12] Dai *et al.* reported the effect of nitrogen functional groups on ruthenium catalysts and found that the modified catalysts exhibited better catalytic activity.[18] Han *et al.* prepared a Ru-based catalyst by using ammonium hexachlororuthenate ($(NH_4)_2RuCl_6$) as the ruthenium precursor, and found that the resulting $(NH_4)_2RuCl_6$/AC catalyst exhibits superior catalytic activity.[24]

For industrial heterogeneous catalysts, especially those used for acetylene hydrochlorination, the stability of the catalyst is also very important. Hydrochlorination is a typical reaction catalyzed by a Lewis acid; however, the strong acidic sites at the surface of the catalyst can cause coke deposition, especially for reactions involving acetylene and olefins. It is known that the Lewis acidity of $RuCl_3$ is much stronger than that of $AuCl_3$ and $HgCl_2$ and the coke deposition phenomenon could be more severe for Ru-based catalysts than Au and Hg catalysts. In addition, according to the literature,[12,15] the main reason for the deactivation of ruthenium catalysts is coke deposition. To inhibit coke deposition, Li *et al.*[13] prepared a series of ruthenium–potassium catalysts to study the

Institute of Industry Catalysis, Zhejiang University of Technology, 18 Chaowang Road, Hangzhou 310014, PR China. E-mail: liying@zjut.edu.cn

† Electronic supplementary information (ESI) available: Fig. S1–S7, Tables S1 and S2, see ESI. See DOI: 10.1039/c8cy01677a

effects of KCl on the performance of Ru-based catalysts. They found that the addition of alkali metals inhibited coke deposition. More importantly, with increasing amount of alkali metal added, the carbon deposition of the catalyst decreased. Li *et al.* studied the effect of ionic liquids on Ru-based catalysts during acetylene hydrochlorination and found that ionic liquids not only increased the amount of HCl adsorbed onto the catalyst but also enhanced HCl activation, which could inhibit self-polymerization of acetylene, which produces coke deposition.[16]

Up to now, there have been no studies investigating the surface acidity of $RuCl_3$/AC catalysts for acetylene hydrochlorination. The present work studied the relationship between the surface acidity and stability of ruthenium catalysts, and provides a simple method to solve the problem of ruthenium catalyst stability by treating the as-prepared $RuCl_3$/AC catalyst with concentrated ammonia solution.

2 Experimental

2.1 Materials

Activated carbon (AC) (coconut carbon, 12–24 mesh) was purchased from Hainan Yeqiu Co., Ltd. Ruthenium chloride hydrate ($RuCl_3{\cdot}3H_2O$) was purchased from Sino-Platinum Metals Co. Ltd. $NH_3{\cdot}H_2O$ (25–28%) was purchased from Hang Zhou Longshan Fine Chemical Co. Ltd. Other reagents were obtained from Shanghai Chemical Reagent Inc. of the Chinese Medicine Group. All materials except for AC were of analytical grade and were used without any further purification. Activated carbon (AC) was washed with a 1 mol L^{-1} HCl solution at 70 °C for 5 hours to remove impurities, followed by washing with water to neutral pH and drying at 120 °C for 5 hours. The dried AC was stored in a desiccator for further use.

2.2 Catalyst preparation

The $RuCl_3$/AC catalyst was prepared using $RuCl_3{\cdot}3H_2O$ as the precursor *via* an incipient impregnation technique. The nominal ruthenium loading was 2 wt%, which was calculated based on Ru metal. The detailed procedure is as follows: 0.29 grams of $RuCl_3{\cdot}3H_2O$ was first dissolved in 8 mL of water, then 5 grams of the activated carbon was added to an aqueous solution of $RuCl_3$ at room temperature. The impregnation was kept at room temperature for 24 hours and then the catalyst was dried at 120 °C for 10 hours. The as-prepared catalyst was denoted as $RuCl_3$/AC. $RuCl_3$/AC was reduced by H_2 with a flow rate of 30 mL min^{-1} at 400 °C for 2 hours. The reduced catalyst was denoted as Ru/AC.

The as-prepared undried $RuCl_3$/AC catalyst was put directly in 8 mL of concentrated $NH_3{\cdot}H_2O$ solution and kept at room temperature for another 24 hours. Then it was dried at 120 °C for 10 hours. The obtained catalyst was denoted as $RuCl_3$-A/AC.

2.3 Measurement of catalytic activity

The catalytic performance was investigated using a fixed-bed glass reactor (i.d. of 10 mm). Acetylene (99.9% purity) was passed through concentrated sulfuric acid solution to remove the trace impurities, and hydrogen chloride gas (99.9% purity) was dried using 5A molecular sieves. Acetylene (3.4 mL min^{-1}) and hydrogen chloride (3.7 mL min^{-1}) were introduced into a heated reactor containing catalyst (2.0 mL) through a mixing vessel *via* calibrated mass flow controllers, giving a C_2H_2 gas hourly space velocity (GHSV) of 100 h^{-1} at 180 °C. The pressure of C_2H_2 and HCl was 0.1 MPa and the feed volume ratio of $V_{HCl}/V_{C_2H_2}$ was 1.10. The microreactor was purged with nitrogen to remove water and air before the reaction. The catalyst was activated by passing HCl gas over it at various times before C_2H_2 and HCl were mixed together. The activation time was 4 hours if not otherwise stated. The reactor effluent was passed through an absorption bottle containing a sodium hydroxide solution to remove the unreacted hydrogen chloride. The gas mixture was analyzed by using a GC-1690F gas chromatograph (GC) equipped with FID detector. The initial conversion of C_2H_2 was recorded after the reaction had proceeded for 1 hour.

2.4 Characterization

X-ray powder diffraction (XRD) measurements were performed by using a Rigaku D/Max-2500/pc powder diffraction system using Cu Kα radiation (40 kV and 100 mA) over the range $10° \leq 2\theta \leq 80°$.

Transmission electron microscope (TEM) images of the samples were obtained using a FEI Tecnai G20 instrument. The samples were mounted and ultrasonically dispersed in ethanol, and then a few droplets of the suspension were deposited on a copper grid coated by a carbon film, followed by drying under ambient conditions.

Nitrogen adsorption isotherms were determined at −196 °C on a Quantachrome Autosorb-IQ apparatus. The samples were outgassed at 350 °C for 3 hours before the adsorption measurements. The specific surface area was obtained by using the Brunauer–Emmett–Teller (BET) model for adsorption data in the relative pressure range of 0.05–0.30. The total pore volume was determined from the aggregation of N_2 vapor adsorbed at a relative pressure of 0.99. The pore size distribution was acquired from the desorption branches of the isotherms using the DFT model.

Hydrogen temperature-programmed reduction (H_2-TPR) of Ru catalysts was carried out with a self-made TPD/TPR instrument. The mass spectra were collected using an online Hiden gas analyzer (QIC 20). Prior to analysis, the samples (*ca.* 50 mg) were placed in a fixed bed U-shaped quartz tubular reactor located inside an electrical furnace. Then each sample was purged at 110 °C for 2 hours in an argon stream to remove the adsorbed water and other impurities on the surface of the sample. After cooling down to room temperature, each sample was heated to 850 °C at a ramp rate of 10 °C min^{-1} under 5 vol% H_2/Ar with a flow rate of 30 mL min^{-1}. The following mass signals were monitored simultaneously on a quadrupole mass spectrometer: m/z = 2, 17, 18, 28, 35, 36, 37, 40 and 44 amu.

Ammonia temperature-programmed desorption (NH_3-TPD) of various Ru catalysts was carried out using a self-made TPD instrument. The mass spectra were collected on an online Hiden gas analyzer (QIC20). Prior to ammonia adsorption, the samples (50 mg) were activated at 120 °C for 1 hour in an argon stream. Subsequently, ammonia was introduced by a stream of 10 vol% NH_3/He at 100 °C. The physically adsorbed NH_3 was removed by purging with an argon steam at 100 °C until the baseline was flat. After cooling down to room temperature, the sample was heated to 500 °C at a ramp rate of 10 °C min^{-1} under argon with a flow rate of 30 mL min^{-1}. The following mass signals were monitored simultaneously using a quadrupole mass spectrometer: m/z = 2, 14, 15, 16, 17, 18, 28, 40 and 44 amu. The quantification of the acidic sites was done by using $(NH_4)_2CO_3$ as a standard compound to calibrate the area of the MS signals.[28]

Thermogravimetric analysis (TGA) was performed using a TG–DTG simultaneous thermal analyzer (NETZSCH STA 449F3) under air at a flow rate of 30 mL min^{-1}. The temperature was increased from 30 °C to 850 °C at a rate of 10 °C min^{-1}.

X-ray photoelectron measurements (XPS) were conducted on a Kratos AXIS Ultra DLD instrument using 300 W Al Kα. The binding energies were calibrated using the contaminant carbon (C 1s 284.6 eV).

3 Results and discussion

3.1 Textural properties and catalytic performance of various Ru catalysts

An incipient impregnation method was used for the preparation of the various carbon-supported catalysts, as shown in Scheme 1. There are three main catalysts studied in this work: $RuCl_3$/AC (as-prepared); Ru/AC (reduced); and $RuCl_3$-A/AC (ammonia pre-treated). For the detailed preparation methods of the catalysts, see the Experimental section.

Table 1 gives the textural properties of the various catalysts prepared by the incipient impregnation method. From Table 1, the surface area and pore volume of activated carbon are 1235 m^2 g^{-1} and 0.53 cm^3 g^{-1}, respectively. The surface area and the pore volume of $RuCl_3$/AC are decreased to 1094 m^2 g^{-1} and 0.47 cm^3 g^{-1}. The decrease of the surface area and pore volume of the AC after impregnation of $RuCl_3$ salts indicates that parts of the pores of AC are filled by $RuCl_3$. Furthermore, the surface area and pore volume of $RuCl_3$-A/AC and Ru/AC are not very different compared to $RuCl_3$/AC. The ruthenium loading values of $RuCl_3$/AC, Ru/AC and $RuCl_3$-A/AC are 2.01%, 2.01% and 2.04%, respectively, as measured using ultraviolet spectrophotometry. This is nearly the same as the theoretical ruthenium loading, indicating that there is no loss of ruthenium during impregnation.

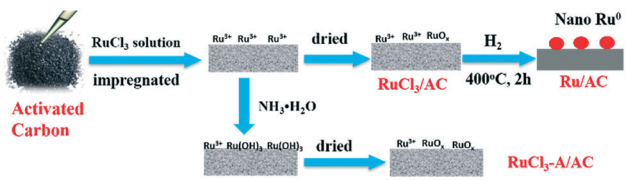

Scheme 1 The preparation process of various ruthenium catalysts.

Fig. 1A and B give the catalytic performances of these Ru-based catalysts for acetylene hydrochlorination. The initial acetylene conversion of $RuCl_3$-A/AC is 82.5%, and acetylene conversion reaches the maximum value of 95.8% after the reaction has proceeded for 8 hours. Meanwhile, the initial acetylene conversion for the $RuCl_3$/AC catalyst reaches the maximum value of 94.0% at the very beginning of the reaction. This existence of an induction period for a catalyst may indicate that the active ruthenium species are formed during the reaction.

To further identify the induction period of the $RuCl_3$-A/AC catalyst, Fig. S1A† shows the effect of HCl activation time on the catalytic performance of $RuCl_3$-A/AC. The induction period was greatly suppressed when the activation time was 6 hours. The initial acetylene conversion for $RuCl_3$-A/AC increased up to the maximum value of 97.2%. This indicates that the active species was generated during pre-treatment with HCl. This result indicates that the active ruthenium species for the ruthenium catalysts is ruthenium chloride. To further identify the active species, Ru/AC (*in situ* reduction of $RuCl_3$/AC in fixed-bed glass reactor) was tested as a comparison and the results are given in Fig. 1B. The initial activity for Ru/AC was only 10%, which is close to the catalytic performance of the carbon support (shown in Fig. 1B). This indicates that metallic Ru is not the active species. The acetylene conversion increased up to 30% in 20 hours and stabilized at 30% after 20 hours. This indicates that the active species was formed during the reaction. The stabilized activity of Ru/AC is still much lower than that of $RuCl_3$/AC and $RuCl_3$-A/AC, although they have similar Ru loadings. This could be due to the fact that Ru nanoparticles are formed during reduction by hydrogen. The Ru dispersion of Ru/AC was determined *via* CO chemisorption to be only 35%, and only the surface Ru atoms could be activated into the active species ($RuCl_3$). Meanwhile for $RuCl_3$/AC,

Table 1 Textural properties of activated carbon and various fresh and used ruthenium catalysts

	Fresh			Used					
Samples	Ru (wt%)	S.A. (m^2 g^{-1})	P.V. (cm^3 g^{-1})	Ru (wt%)	S.A. (m^2 g^{-1})	P.V. (cm^3 g^{-1})	Amount of coke deposition (%)	Acid content (mmol g^{-1})	Deactivation rate (% h^{-1})
AC	~	1235	0.53		—	—	—	—	—
$RuCl_3$/AC	2.01	1094	0.47	1.80	22	0.02	11.6	6.34	1.64
$RuCl_3$-A/AC	2.04	1102	0.47	1.88	340	0.17	9.1	2.66	0.14
Ru/AC	2.01	1105	0.47	2.00	946	0.41	Not detected	None	None

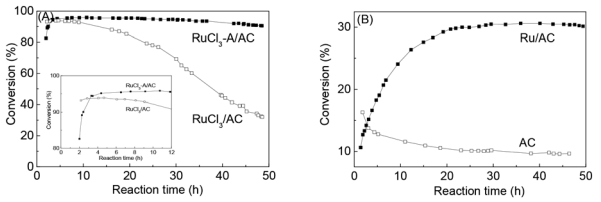

Fig. 1 The conversion of acetylene in acetylene hydrochlorination over (A) $RuCl_3$/AC and $RuCl_3$-A/AC and (B) AC and Ru/AC catalysts. Reaction conditions: T = 180 °C, GHSV(C_2H_2) = 100 h^{-1} and $V_{HCl}/V_{C_2H_2}$ = 1.10.

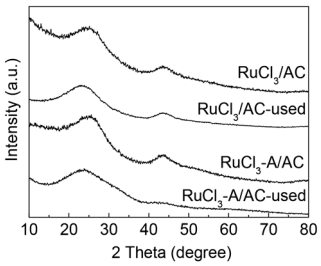

Fig. 2 XRD patterns of $RuCl_3$/AC, $RuCl_3$/AC-used, $RuCl_3$-A/AC and $RuCl_3$-A/AC-used catalysts.

monolayer $RuCl_3$ can be easily formed on the surface of the activated carbon support according to the spontaneous dispersion phenomenon reported by Xie *et al.*[29,30] From Fig. 1A, it can be clearly seen that the deactivation rate is obviously decreased for $RuCl_3$-A/AC compared with $RuCl_3$/AC. The acetylene conversion of the $RuCl_3$-A/AC catalyst is still above 90.5% after the catalyst has been used for 50 h. The deactivation rates for $RuCl_3$-A/AC and $RuCl_3$/AC are 0.14% h^{-1} and 1.64% h^{-1} respectively. This result indicates that the ammonia pretreatment of the as-prepared $RuCl_3$/AC catalyst can greatly improve the stability. To identify the role of ammonia pretreatment and the deactivation mechanism of the ruthenium catalysts, a detailed characterization of the textural properties and statuses of the Ru species in these two catalysts are given and discussed below.

3.2 Characterization of the fresh and used $RuCl_3$/AC and $RuCl_3$-A/AC catalysts

Fig. S2A and B† show the isotherms and pore size distributions of the fresh and used Ru catalysts. The isothermal curves for the fresh $RuCl_3$/AC and $RuCl_3$-A/AC catalysts are type IV with an H4 hysteresis loop in a high relative pressure range, which indicates that these samples have mesoporous structures in addition to a micropore structure. The pore size distributions of all the samples calculated *via* DFT methods are given in Fig. S2B.† All the samples have main pore size distributions in the range of 0.5–5.0 nm. For $RuCl_3$/AC-used, the isothermal curve becomes flat without any hysteresis loops, indicating that both micropores and mesopores have been blocked. For $RuCl_3$-A/AC-used, the isothermal curve is also changed. However, from the pore size distribution, the main micropores and mesopores still exist. The textural properties of the fresh and used catalysts are summarized in Table 1. The specific surface area and pore volume of $RuCl_3$/AC-used and $RuCl_3$-A/AC-used are greatly decreased.

Fig. 2 displays the XRD patterns of the fresh and used catalysts. There are only two diffraction peaks at 26.5° and 45° for all the fresh and used catalysts, which can be assigned to the (002) and (101) diffraction peaks of amorphous carbon. No discernible reflection is detected for all the fresh and used Ru catalysts, indicating that the ruthenium species are highly dispersed and the particle size is less than 4 nm and no aggregation of $RuCl_3$ occurs even after the reaction has proceeded for 50 hours.

The STEM and HRTEM images are also provided in Fig. 3 and S3,† respectively. There are no Ru nanoclusters or particles observed at high resolution mode. Even after the reaction, there are still no Ru nanoparticles to be observed. However, from the scanning transmission electron mode, the distribution of Ru element is clearly observed. This might indicate a monolayer distribution of $RuCl_3$ salts on the surface of the activated carbon.

Fig. 4 shows hydrogen temperature-programmed reduction profiles of the fresh and used Ru-based catalysts. Compared with the Ru catalysts, activated carbon shows very weak H_2 consumption (see ESI† Fig. S4†). For $RuCl_3$/AC, there are two peaks of H_2 consumption located at 140 °C and 235 °C. Combined with a signal at m/z = 18 corresponding to H_2O, it is concluded that the consumption of H_2 is related to the reduction of $RuCl_3$ and RuO_x. However, no peaks corresponding to HCl are detected due to the re-adsorption of HCl on the carbon support. For $RuCl_3$-A/AC, there are two peaks of H_2 consumption located at 180 °C and 270 °C that correspond to $RuCl_3$ and RuO_x. Obviously, the temperature of the Ru reduction peak is shifted to high temperature and the amount of ruthenium oxide is increased. This indicates that the treatment with ammonia solution can change the status of $RuCl_3$ species and increase the amount of ruthenium oxides. For both the used $RuCl_3$/AC and $RuCl_3$-A/AC catalysts, the H_2 consumption peak shifts to 325 °C and there is an

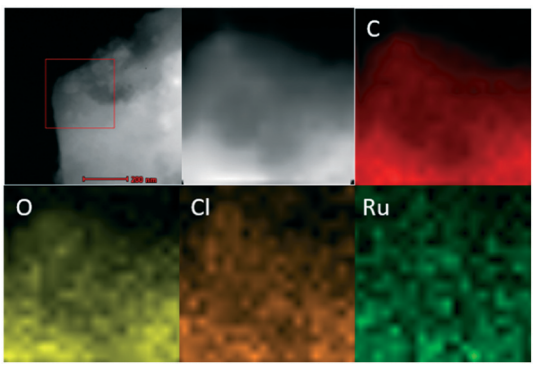

Fig. 3 STEM images and element mapping for the $RuCl_3$-A/AC catalyst.

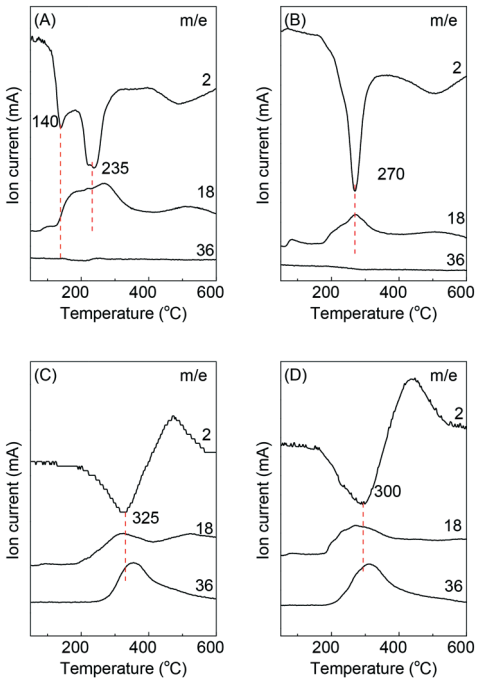

Fig. 4 H_2-TPR profiles of (A) $RuCl_3$/AC, (B) $RuCl_3$-A/AC (C) $RuCl_3$/AC-used and (D) $RuCl_3$-A/AC-used catalysts.

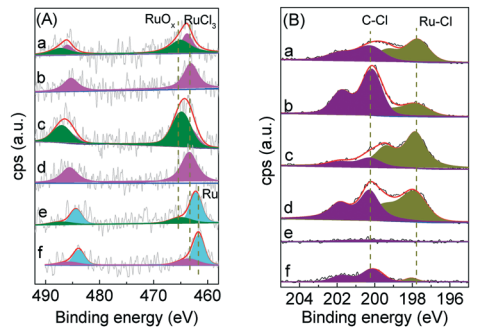

Fig. 5 XPS spectra of (a) $RuCl_3$/AC, (b) $RuCl_3$/AC-used, (c) $RuCl_3$-A/AC, (d) $RuCl_3$-A/AC-used catalysts, (e) Ru/AC, and (f) Ru/AC-used, for (A) Ru 3p and (B) Cl 2p.

obvious HCl peak detected. This indicates that the Ru species on the catalyst has been changed into $RuCl_3$ species during the reaction. The reduction temperature of the used catalyst, which is shifted to a high temperature, is due to surface coke deposition, which can inhibit the reduction of ruthenium.

X-ray photoelectron spectroscopy (XPS) was used to characterize the status of the ruthenium species on the catalysts. Because the binding energy of the Ru 3d orbital overlaps with that of C 1s, the Ru 3p orbital was chosen for the analysis.[31,32] The high-resolution Ru 3p spectra for the fresh and used $RuCl_3$/AC, $RuCl_3$-A/AC and Ru/AC catalysts are given in Fig. 5A. The deconvolution results, including the binding energy and relative content of different peaks, are shown in Table 2. The photoelectron spectra of Ru 3p for fresh Ru/AC, $RuCl_3$/AC and $RuCl_3$-A/AC catalysts clearly show two doublet-peaks. The spin–orbit splitting of Ru 3p is 22.2 eV and intensity ratio is about 2 : 1 (Ru $3p_{3/2}$: Ru $3p_{1/2}$). For $RuCl_3$/AC, around 44% of the ruthenium is ascribed to Ru^{3+} species in $RuCl_3$ (463.4 eV)[33] and around 55.9% of ruthenium is ascribed to $Ru^{\sigma+}$ species in RuO_x (465.0 eV).[34] For $RuCl_3$-A/AC, around 32.5% of ruthenium was ascribed to Ru^{3+} species in $RuCl_3$ (463.4 eV) and around 67.5% of ruthenium was ascribed to $Ru^{\sigma+}$ species in RuO_x (464.8 eV). For Ru/AC, around 75.3% of ruthenium was ascribed to Ru^0 species (462.2 eV)[35] and around 24.7% of ruthenium was ascribed to $Ru^{\sigma+}$ species in RuO_x (465.0 eV). The RuO_x species is present in the Ru/AC catalyst, which may be because the Ru/AC catalyst was exposed to air and became oxidized. For the $RuCl_3$/AC-used and $RuCl_3$-A/AC-used catalysts, the main peak of Ru $3p_{3/2}$ at 463.4 eV is attributed to Ru^{3+} species in $RuCl_3$ and there are apparently no Ru^0 and RuO_x species for both samples. However, for the Ru/AC-used catalyst, around 72.2% of ruthenium was ascribed to Ru^0 species (461.7 eV) and around 27.8% of ruthenium was ascribed to Ru^{3+} species in $RuCl_3$ (463.6 eV). This indicates that some of Ru^0 has been oxidized to $RuCl_3$ under the reaction conditions and the $RuCl_3$ species is the active center of the Ru-based catalysts. This result is consistent with the induction period for these catalysts as discussed in a previous paragraph.

The XPS spectra of Cl 2p for fresh and used Ru-based catalysts are given in Fig. 5B. The Cl 2p spectra could be split into doublet-peaks (Cl $2p_{3/2}$ and Cl $2p_{1/2}$), with the energy separation being 1.6 eV and the intensity ratio being 2 : 1. Therefore, the Cl 2p peaks are fitted into two peaks according to the composition of the ruthenium catalyst. The peak located at 197.7 ± 0.1 eV is closer to the binding energy of Cl 2p species in $RuCl_3$.[36] The peak at 200.2 ± 0.1 eV is assigned to C–Cl,[37] which may be formed by the chemical adsorption of Cl^- anions produced by the hydrolysis of $RuCl_3$ in aqueous solution (see ESI† Fig. S5†). The ratio of these two species is 42.4% and 57.6% for $RuCl_3$/AC, and 16.3% and 83.7% for

Table 2 The XPS spectra fitting results of Ru 3p and Cl 2p for the fresh and used ruthenium catalysts

	Ru 3p (area%)			Cl 2p (area%)	
Samples	Ru (462.2 eV)	$RuCl_3$ (463.4 eV)	RuO_x (465.0 eV)	C : Cl (200.2 eV)	Ru : Cl (197.7 eV)
$RuCl_3$/AC	—	44.1	55.9	42.4	57.6
$RuCl_3$/AC-used	—	100	—	73.8	26.2
$RuCl_3$-A/AC	—	32.5	67.5	16.3	83.7
$RuCl_3$-A/AC-used	—	100	—	48.4	51.6
Ru/AC	75.3	—	24.7	100	0
Ru/AC-used	72.2	27.8	—	86.0	14.0

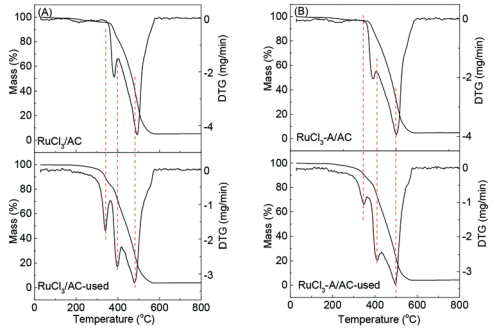

Fig. 6 TG and DTG curves of (A) $RuCl_3$/AC and $RuCl_3$/AC-used; (B) $RuCl_3$-A/AC and $RuCl_3$-A/AC-used catalysts under air flow.

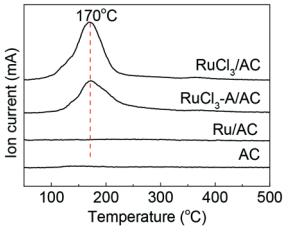

Fig. 7 NH_3-TPD profiles of AC, Ru/AC, $RuCl_3$/AC, and $RuCl_3$-A/AC catalysts.

$RuCl_3$-A/AC, respectively. This indicates that the addition of ammonia during impregnation greatly affected the hydrolysis behavior of $RuCl_3$. It should be noted that after the reaction had proceeded for 50 hours, the C : Cl ratio greatly increased, both for the $RuCl_3$/AC-used and $RuCl_3$-A/AC-used catalysts. This indicates that the coke deposition occurs for the used catalysts and is caused by vinyl chloride polymerization. However, it can be clearly seen that the coke deposition for $RuCl_3$/AC-used is much heavier than that of $RuCl_3$-A/AC-used. Comparing Ru/AC with Ru/AC-used, the Ru : Cl ratio for Ru/AC-used increased to 14.0. This result is consistent with the XPS spectra of Ru 3p for Ru/AC.

Fig. 6 gives the thermal gravimetric analysis results of the fresh and used $RuCl_3$/AC and $RuCl_3$-A/AC catalysts under air flow. For both the fresh $RuCl_3$/AC and $RuCl_3$-A/AC catalysts, there are two weight loss peaks at 380 °C and 490/500 °C. The first peak can be assigned to the combustion of carbon species around Ru species, which can be catalyzed by ruthenium. The second peak at the higher temperature (490–500 °C) is due to the combustion of the carbon support. A new peak appears at 340 °C for the used $RuCl_3$/AC and $RuCl_3$-A/AC catalysts. This can be assigned to the combustion of the deposited carbon species. Therefore, the amount of coke deposition is calculated based on the weight loss in the temperature range of 150–380 °C. The amount of coke deposition for the $RuCl_3$/AC catalyst is about 11.6% and 9.1% for the $RuCl_3$-A/AC catalysts (listed in Table 1). The loadings of ruthenium for $RuCl_3$/AC-used and $RuCl_3$-A/AC-used catalysts are 1.80% and 1.88% (given in Table 1). Considering the weight increase caused by coke deposition of the used catalyst, there was almost no loss of ruthenium. Therefore, the main cause of catalyst deactivation is coke deposition.

To identify the differences between the $RuCl_3$/AC and $RuCl_3$-A/AC catalysts, NH_3 temperature-programmed desorption was used to characterize the surface acidity of the catalysts. The results are given in Fig. 7. Both Ru/AC and AC were also characterized for comparison. For $RuCl_3$/AC and $RuCl_3$-A/AC, there is only a NH_3 desorption peak at 170 °C. It also can be seen that the peak area of the $RuCl_3$-A/AC catalyst is smaller than that of the $RuCl_3$/AC catalyst. Furthermore, Ru/AC and activated carbon have no ammonia desorption peak. The above results indicate that the acidic sites are generated by $RuCl_3$ species on the surface of the catalysts. The concentrations of acidic sites are 6.34 mmol g^{-1} for $RuCl_3$/AC and 2.66 mmol g^{-1} for $RuCl_3$-A/AC. The treatment with ammonia solution can greatly reduce the amount of surface acidic sites on the ruthenium catalysts. This result explains the different deactivation rates of these catalysts. To exclude the effect of the ammonia treatment on the activated carbon, an ammonia-treated activated carbon was used as a reference to prepare a $RuCl_3$/AC-A catalyst. The catalytic performance and NH_3-TPD results are provided in Fig. S6.† The stability of the $RuCl_3$/AC-A is slightly better than $RuCl_3$/AC, but it is still far lower than that of the $RuCl_3$-A/AC catalyst. This can be explained by the acidity difference between AC and $RuCl_3$/AC. Compared with $RuCl_3$, the acidity of activated carbon is quite low. The main acidity is generated by $RuCl_3$. Therefore, the ammonia treatment of the carbon support is not as obvious as the treatment of the as-prepared catalysts.

From the above analysis, we concluded that coke deposition, caused by the surface acidity of the $RuCl_3$/AC catalyst, is the main reason for the deactivation of the catalyst. Combined with the TPR and XPS characterizations, RuO_x may be formed during the ammonia treatment. The following reaction may occur during the ammonia treatment of the as-prepared catalysts: $RuCl_3 + NH_3{\cdot}H_2O \rightarrow Ru(OH)_3\downarrow + NH_4Cl$. Ru ions can precipitate in the form of hydroxide facilely because the $K_{sp}(Ru(OH)_3)$ is as low as 1×10^{-36} (25 °C). This has been fully discussed in our previous reports.[38] The existence and decomposition of $Ru(OH)_3$ results in the content of RuO_x being greatly enhanced. Therefore, the present study not only points out the deactivation mechanism of the carbon-supported ruthenium chloride but also gives an easy and efficient approach to solve the problem of deactivation. However, as shown in the data in Table S1,† the catalytic performance of the $RuCl_3$-A/AC catalyst is not the highest compared with the data reported by Li *et al.*,[17] and therefore needs to be improved in future. The improvement of the catalytic activity can be done by increasing of the dispersion of ruthenium, such as trying to prepare single-atom catalysts or by adjusting the metal support interaction to increase the intrinsic activity of the active sites.

4 Conclusions

In summary, we prepared a stable $RuCl_3$-A/AC catalyst by applying a simple ammonia treatment during an impregnation process. From the catalyst characterization results, the $RuCl_3$ species was identified as the active species, and the surface

acidity of $RuCl_3$/AC catalyst is generated mainly from $RuCl_3$ species, which can easily cause coke deposition. The enhancement of the stability of $RuCl_3$-A/AC is attributed to the formation of RuO_x species and the decrease of the surface acidity. The present work identifies the deactivation mechanism of ruthenium-based catalysts and offers a simple way to prepare mercury-free catalysts with extraordinary stability for acetylene hydrochlorination. However, the activity of the ruthenium catalyst needs to be further improved.

Conflicts of interest

There are no conflicts to declare.

Acknowledgements

The financial support from Natural Science Foundation of Zhejiang Province (LY17B030010) is gratefully acknowledged.

Notes and references

1 H. Schobert, *Chem. Rev.*, 2014, **114**, 1743–1760.
2 T. Degnan, *Focus on Catalysts*, 2016, **3**, 1–2.
3 M. Zhu, Q. Wang, K. Chen, Y. Wang, C. Huang, H. Dai, F. Yu, L. Kang and B. Dai, *ACS Catal.*, 2015, **5**, 5306–5316.
4 J. Zhong, Y. Xu and Z. Liu, *Green Chem.*, 2018, **20**, 2412–2427.
5 P. Johnston, N. Carthey and G. Hutchings, *J. Am. Chem. Soc.*, 2016, **47**, 14548–14557.
6 G. Malta, S. Kondrat, S. Freakley, C. Davies, L. Lu, S. Dawson, A. Thetford, E. Gibson, D. Morgan and W. Jones, *Science*, 2017, **355**, 1399–1403.
7 J. Zhao, B. Wang, X. Xu, Y. Yu, S. Di, H. Xu, Y. Zhai, H. He, L. Guo, Z. Pan and X. Li, *J. Catal.*, 2017, **350**, 149–158.
8 D. Hu, L. Wang, F. Wang and J. Wang, *Catal. Commun.*, 2018, **115**, 45–48.
9 J. Liu, G. Lan, Y. Qiu, X. Wang and Y. Li, *Chin. J. Catal.*, 2018, **39**, 1664–1671.
10 M. Zhu, L. Kang, Y. Su, S. Zhang and B. Dai, *Can. J. Chem.*, 2013, **91**, 120–125.
11 Y. Han, M. Sun, W. Li and J. Zhang, *Phys. Chem. Chem. Phys.*, 2015, **17**, 7720–7730.
12 J. Zhang, W. Sheng, C. Guo and W. Li, *RSC Adv.*, 2013, **3**, 21062–21068.
13 Y. Jin, G. Li, J. Zhang, Y. Pu and W. Li, *RSC Adv.*, 2015, **5**, 37774–37779.
14 J. Xu, J. Zhao, T. Zhang, X. Di, S. Gu, J. Ni and X. Li, *RSC Adv.*, 2015, **5**, 38159–38163.
15 H. Zhang, W. Li, Y. Jin, W. Sheng, M. Hu, X. Wang and J. Zhang, *Appl. Catal., B*, 2016, **189**, 56–64.
16 Y. Li, Y. Dong, W. Li, Y. Han and J. Zhang, *Mol. Catal.*, 2017, **443**, 220–227.
17 S. Shang, W. Zhao, Y. Wang, X. Li, J. Zhang, Y. Han and W. Li, *ACS Catal.*, 2017, **7**, 3510–3520.
18 N. Xu, M. Zhu, J. Zhang, H. Zhang and B. Dai, *RSC Adv.*, 2015, **5**, 86172–86178.
19 G. Li, W. Li, H. Zhang, Y. Pu, M. Sun and J. Zhang, *RSC Adv.*, 2015, **5**, 9002–9008.
20 L. Hou, J. Zhang, Y. Pu and W. Li, *RSC Adv.*, 2016, **6**, 18026–18032.
21 W. Zhao, W. Li and J. Zhang, *Catal. Sci. Technol.*, 2016, **6**, 1402–1409.
22 B. Man, H. Zhang, J. Zhang, X. Li, N. Xu, H. Dai, M. Zhu and B. Dai, *RSC Adv.*, 2017, **7**, 23742–23750.
23 G. Lan, Y. Yang, X. Wang, W. Han, H. Tang, H. Liu and Y. Li, *Microporous Mesoporous Mater.*, 2018, **264**, 248–253.
24 J. Gu, Y. Gao, J. Zhang, W. Li, Y. Dong and Y. Han, *Catalysts*, 2017, **7**, 17.
25 B. Man, H. Zhang, C. Zhang, X. Li, H. Dai, M. Zhu, B. Dai and J. Zhang, *New J. Chem.*, 2017, **41**, 14675–14682.
26 X. Li, H. Zhang, B. Man, L. Hou, C. Zhang, H. Dai, M. Zhu, B. Dai, Y. Dong and J. Zhang, *Catalysts*, 2017, **7**, 311.
27 Y. Pu, J. Zhang, L. Yu, Y. Jin and W. Li, *Appl. Catal., A*, 2014, **488**, 28–36.
28 L. Rodríguez-González, F. Hermes, M. Bertmer, E. Rodríguez-Castellón, A. Jiménez-López and U. Simon, *Appl. Catal., A*, 2007, **328**, 174–182.
29 Y. Xie, F. Yang, J. Liu and Q. Tang, *Sci. Sin., Ser. B*, 1982, **8**, 3–12.
30 X. Yu, N. Wu, H. Huang, Y. Xie and Y. Tang, *J. Mater. Chem.*, 2001, **11**, 3337–3342.
31 Z. Bo, D. Hu, J. Kong, J. Yan and K. Cen, *J. Power Sources*, 2015, **273**, 530–537.
32 V. Costa, M. Jacinto, L. Rossi, R. Landers and E. Gusevskaya, *J. Catal.*, 2011, **282**, 209–214.
33 C. Takoudis, M. Weaver and H. Chan, *J. Catal.*, 1997, **172**, 336–345.
34 J. Ma, Y. Feng, J. Yu, D. Zhao, A. Wang and B. Xu, *J. Catal.*, 2010, **275**, 34–44.
35 J. Gómez de la Fuente, M. Martínez-Huerta, S. Rojas, P. Hernández-Fernández, P. Terreros, J. Fierro and M. Peña, *Appl. Catal., B*, 2009, **88**, 505–514.
36 I. Pollini, *Phys. Rev. B: Condens. Matter Mater. Phys.*, 1994, **50**, 2095–2103.
37 J. Wang, B. Deng, H. Chen, X. Wang and J. Zheng, *Environ. Sci. Technol.*, 2009, **43**, 5223–5228.
38 Y. Li, C. Pan, W. Han, H. Chai and H. Liu, *Catal. Today*, 2011, **174**, 97–105.